JOURNAL OF MATERIALS SCIENCE 29 (1994) 4027–4036

Microstructure and mechanical properties of pitch-based carbon fibres

YANLING HUANG, R. J. YOUNG
Manchester Materials Science Centre, UMIST/University of Manchester, Grosvenor Street, Manchester M1 7HS, UK

The microstructure of a series of mesophase pitch-based carbon fibres have been examined using X-ray diffraction, electron microscopy and Raman spectroscopy. It has been shown that the mechanical properties of the fibres are related directly to the response of this microstructure to deformation and, in particular, that the Young's modulus and tensile strength of the fibres are controlled directly by the fibre microstructure. It has also been shown that Raman spectroscopy can be a useful technique for not only characterizing the microstructure of the fibres but also for following molecular deformation in the fibres. It was found that the position of the 1580 cm^{-1} Raman band for the fibres shifted with the application of stress and that the rate of shift per unit strain was proportional to the Young's modulus of the fibres. It was also shown that this reflected the higher degree of stressing of the graphite plane in the higher modulus fibres, consistent with recently developed theories which attempt to explain the dependence of the mechanical properties of carbon fibres upon the degree of orientation of the graphite planes.

1. Introduction

Over the past decade there has been considerable research effort in producing carbon fibres more economically and with improved mechanical properties. Mesophase pitch-based carbon fibres represent a major success in this area [1–4]. Anisotropic mesophase pitch has the advantage of good graphitizing characteristics and employing it allows the production of a high yield of carbon fibres at relatively low cost. Carbon fibres produced from mesophase pitch can have Young's moduli as high as 830 GPa which is close to the value of 1000 GPa expected for crystalline graphite [5]. High-modulus rayon-based or PAN-based carbon fibres with moduli values in the region of 500–700 GPa may only be produced by employing an expensive hot-stretching process [6, 7] or by boron doping [8].

Mesophase pitch-based carbon fibres have been shown, by using high-resolution scanning electron microscopy (HRSEM), to have a sheet-like microstructure [9]. Guigon and Oberlin [10] found that mesophase pitch-based fibres consisted of a combination of three-dimensionally ordered graphite crystals, turbostratic graphite and porous domains. Endo [11] also found evidence for a three-dimensionally ordered graphitic structure using a combination of X-ray diffraction and electron microscopy. Another characteristic feature of the microstructure of pitch-based carbon fibres is their wide variety of transverse structures such as the onion-skin, radially-oriented and oriented-core types or even mixtures of these structures [12, 13]. Matsumoto [14] found that this transverse structure is controlled by the shear-spinning conditions in the spinneret and the dimensions of the die.

In this paper the microstructure of a series of mesophase pitch-based carbon fibres, studied using a combination of X-ray diffraction, optical microscopy, electron microscopy and Raman spectroscopy in an attempt to obtain a full understanding of the relationship between the mechanical properties and microstructure of the fibres is described.

2. Experimental procedure

2.1. Materials

The principal materials used in the study were P-series mesophase pitch-based carbon fibres from Amoco, from the same batch that have been investigated elsewhere [9]. Two other pitch-based fibres were also examined. They were fibre S1 (Idemitsu Kosan Co., Japan) which has good tensile strength, and fibre C700 (Du Pont) which has superior thermal and electrical conductivities. Some mechanical and structural properties quoted by the manufacturers for the fibres are given in Table I.

2.2. Structural characterization

Wide angle X-ray diffraction (WAXD) traces were obtained from ground-up samples of the fibres using a Philips PW 1710 diffractometer and CuK_α radiation. About 10% of silicon powder was mixed with the samples for reference purposes. The *d*-spacings and crystalline sizes along the **a**- and **c**-crystal directions were determined using the Scherrer equation from the

0022–2461

TABLE I Mechanical and physical properties of the carbon fibres (manufacturers' data)

Fibre	Tensile modulus (GPa)	Tensile strength (GPa)	Density (g cm^{-3})
P25	158	1.38	1.90
P55	379	1.90	2.00
P75	517	2.07	2.04
P100	724	2.24	2.15
P120	827	2.24	2.18
S1	235	2.94	2.00
C700	827	2.21	2.13

positions of the diffraction maxima and the width at half-maximum intensity of the (0 0 2), (1 0) and (1 1) peaks.

Fracture surfaces of the fibres were observed uncoated using a JEOL JSM 6300F field emission SEM. It was found to be capable of resolving the fine structure of the carbon fibres at high magnification using relatively low voltages, in the range 2–5 kV. Fracture surfaces of the carbon fibres were also examined after tensile testing using a conventional SEM (Philips 505) operated at 20 kV.

Specimens were prepared for transmission electron microscopy (TEM) by bonding a single layer of carbon fibres on to a single holed copper disc. The disc was then thinned to electron transparency in an Ion Tech 791 ion beam thinner using an argon ion beam at 5 kV and 0.1 mA with an angle 17° to the fibre surface. TEM was undertaken on the thinned sections using an analytical electron microscope (Philips 400T) operated at an accelerating voltage of 120 kV. Bright- and dark-field images and selected-area electron diffraction (SAD) patterns were obtained for several fibres.

2.3. Mechanical testing

The tensile modulus and tensile strength of the fibres were determined using a single-filament tensile test. Single fibres were mounted on paper cards using a slow-setting epoxy resin adhesive at room temperature which was left to cure for 24 h at room temperature. The paper cards were mounted between the grips of an Instron 1121 mechanical testing machine. The edges of the cards were cut and the load-elongation curves were recorded on chart paper. Gauge lengths of 10, 25, 50 and 100 mm were used with the cross-head speed adjusted to give an initial strain rate of 0.02 min^{-1} and a 0.5 N full-scale deflection was employed. At least 15 specimens were tested for each gauge length and the fibre strain was determined from the cross-head displacement. The fibre diameters were measured using an Olympus optical microscope connected to an image analyser and the stress on each fibre was determined from the load. Due to the difficulties in specimen preparation and testing, single fibre mechanical tests on fibres P100, P120 and C700 could not be undertaken and manufacturers' data had to be used.

2.4. Raman spectroscopy

Raman spectra were obtained from single carbon fibres with and without stress using a Raman microprobe system. This consisted of a modified optical microscope coupled to a Spex 1403 double monochromator. The fibres were mounted on a small straining rig using aluminium tabs and cyanoacrylate adhesive. The gauge length of the fibres was ca. 15 mm and the fibre axis was aligned parallel to the stretching direction to within ± 5°. The displacements of the fibres were determined to an accuracy of ± 5 μm using the micrometer attached to the straining rig. Raman spectra were excited using the 488 nm line of an argon ion laser operated at 10 mW (ca. 1 mW at the fibre) and the laser beam was polarized parallel to the fibre axis for all measurements. The Raman spectra were recorded using a liquid N_2 cooled charge coupled device (CCD) detector and then analysed using a Lorentzian fitting procedure to determine the band intensity, band width and band position.

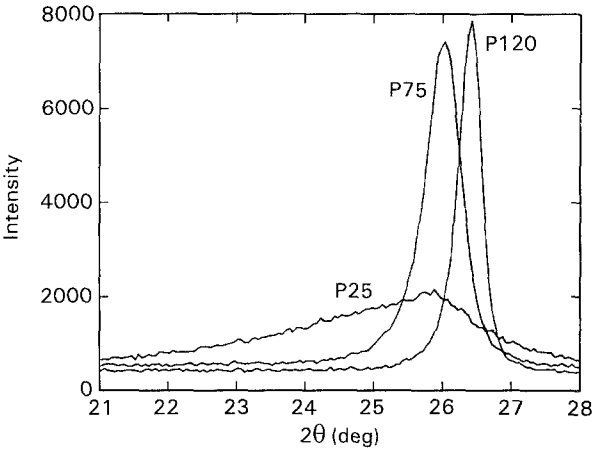

Figure 1 WAXD patterns of fibres P25, P75 and P120 in the 2θ range of 21–28°.

3. Results and discussion

3.1. Fibre structure

3.1.1. X-ray diffraction

Wide-angle X-ray diffraction patterns of ground-up fibres of P25, P75 and P120 for 2θ values in the range of 21–28° are presented in Fig. 1 and show well-defined (0 0 2) peaks at ca. 2θ = 26°. However, in the case of P25, the (0 0 2) peak is asymmetric and there is a long tail on the low-angle side indicating a certain amount of disorder in the structure. The (1 0) peak at 2θ = 42–44° was less well defined. In the case of the lower modulus fibres P25, P55, P75 and S1 it appeared as a broad band characteristic of a turbostratic two-dimensionally ordered structure [1 1], whereas in the case of P100, P120 and C700 it could be resolved into two peaks, (1 0 0) and (1 0 1), suggesting the presence of three-dimensional crystal order.

The (0 0 2) *d*-spacing and crystal sizes along the **a**- and **c**-directions, L_a and L_c, are listed in Table II for all the fibres. It can be seen that the *d*-spacing for fibres P120 and C700 is close to the ideal value for graphite of 0.335 nm, corresponding to the spacing of close-packed sheets in a perfect graphite crystal. This indicates that the two fibres are both highly graphitized. In contrast, the values of the *d*-spacing increases with decreasing fibre modulus going from P120 to P25,

TABLE II Structural parameters determined by X-ray diffraction and TEM

Fibre	Diameter (μm)	d-spacing (nm)	L_a (nm)	L_c (nm)	θ_h (°)
P25	11.5	0.344	5.7	3.2	19.2
P55	10.6	0.342	11.0	16.2	11.6
P75	10.7	0.341	11.4	19.6	10.1
P100	10.5	0.339	43.0	29.1	6.4
P120	11.1	0.337	45.7	37.2	4.8
S1	11.3	0.351	6.0	3.2	14.3
C700	10.2	0.337	45.7	37.2	5.0

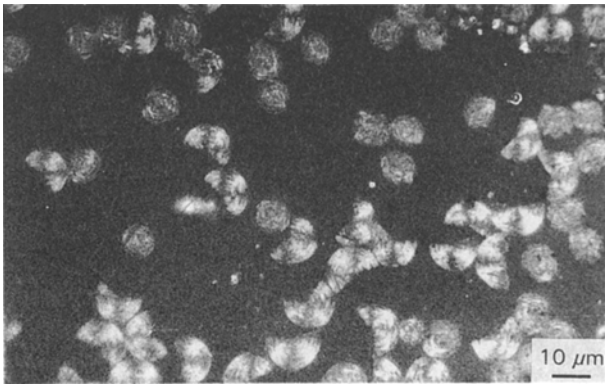

Figure 2 Polarized-light optical micrograph of a polished section of a number of embedded P120 fibres.

indicative of a turobstratic structure and a decreasing degree of graphitization. The increasing values of L_a and L_c with increasing fibre modulus are consistent with this interpretation.

3.1.2. Optical microscopy

The polished cross-sections of fibres embedded in an epoxy resin were viewed under polarized light in an optical microscope and they were seen to be generally circular in shape. Fig. 2 shows the cross-sections of high-modulus P120 fibres and it can be seen that there is a significant variation of fibre diameter in the batch of fibres sectioned. Moreover, it can be seen that the smaller diameter fibres have a random structure whereas the larger diameter ones show well-defined extinction patterns indicative of a radially-oriented structure. In addition, it appears that these fibres tend to split easily along their length into half or quarter fibres, consistent with the appearance of their microstructure. The average diameters of the fibres are listed in Table II, although significant variations in diameter were found, especially for fibres P75, P100, P120 and C700. For example, fibres of P75 were found to have diameters in the range 8.0–13.8 μm with an average of 10.7 μm.

3.1.3. Scanning electron microscopy

Fracture surfaces of the P-series of pitch-based carbon fibres are shown in Fig. 3, they all appear to have a sheet-like structure to some extent. In P25 the graphite sheets appear to be poorly defined, highly curved and rather random in orientation. In P55 and P75 the sheets are radially-oriented in the skin regions but random in the core of the fibres. In the case of P100 and P120 the sheets are mainly radially-oriented, but for P120 at least two types of transverse structure can be observed, as shown in Fig. 3. One type of structure has the sheets radiating out of the fibre centre, whereas the other is an oriented-core type of structure. These differences in microstructures for P120 are consistent with the optical microscope observations in Fig. 2.

3.1.4. Transmission electron microscopy

Fig. 4 shows SAD patterns of ion-beam thinned sections of the fibres P25, P75 and P120. The differences in the arcing and definition of the equatorial (0 0 2) reflections shows that both the degree of graphitization and level of orientation of the graphite planes increases from P25 to P120 in line with the observed increase in fibre modulus (Table I). The quantitative analysis of patterns has been employed successfully by Young *et al.* [15] to determine the relative degree of orientation in different aramid fibres and differences in the degree of orientation between the skin and core regions of the same fibres. The same approach has been adopted in this study by measuring the distribution of intensity across the (0 0 2) arcs using a microdensitometer [15]. This involved scanning along the equator to determine the position of the (0 0 2) reflection and the baseline, and then scanning in the perpendicular direction to determine the intensity distribution across the (0 0 2) arc. For the lower-modulus fibres the broader intensity distribution across the (0 0 2) arcs was determined using a Magiscan Image Analyser. The half-width at half-maximum intensity θ_h was taken as a measure of the degree of molecular orientation relative to the fibre axis. The values of θ_h for the different fibres are listed in Table II, it can be seen that they range from ca. 19° for the lowest-modulus fibre to $< 5°$ for the highest-modulus fibres. The values of θ_h in Table II have not been corrected for instrumental broadening or instrumental distortion. It was also found that, unlike aramid fibres [15], there were no measurable differences in θ_h between the fibre skin and core regions for the pitch-based fibres within the experimental error in measuring θ_h of $\pm 0.5°$.

Fig. 5a is a bright-field TEM micrograph of fibre P100 showing a typical interlinked fibrillar structure and Fig. 5b is a (0 0 2) dark-field image of a similar region. It can be seen that the microfibrils are mainly parallel to the fibre axis indicating that P100 has a high degree of orientation. There are also long, needle-like voids between the microfibrils with their long axes parallel to the fibre axis. Fine bands which appear dark in the bright-field micrographs and light in the dark-field micrographs can also be seen in the microfibrils oriented perpendicular to the fibre axis. These extinction bands are thought to be due to either a Moiré effect from crossing fibrils [16] or lattice distortion [17]. Since the fibres have a radially-oriented structure the electron beam is parallel to the edge of

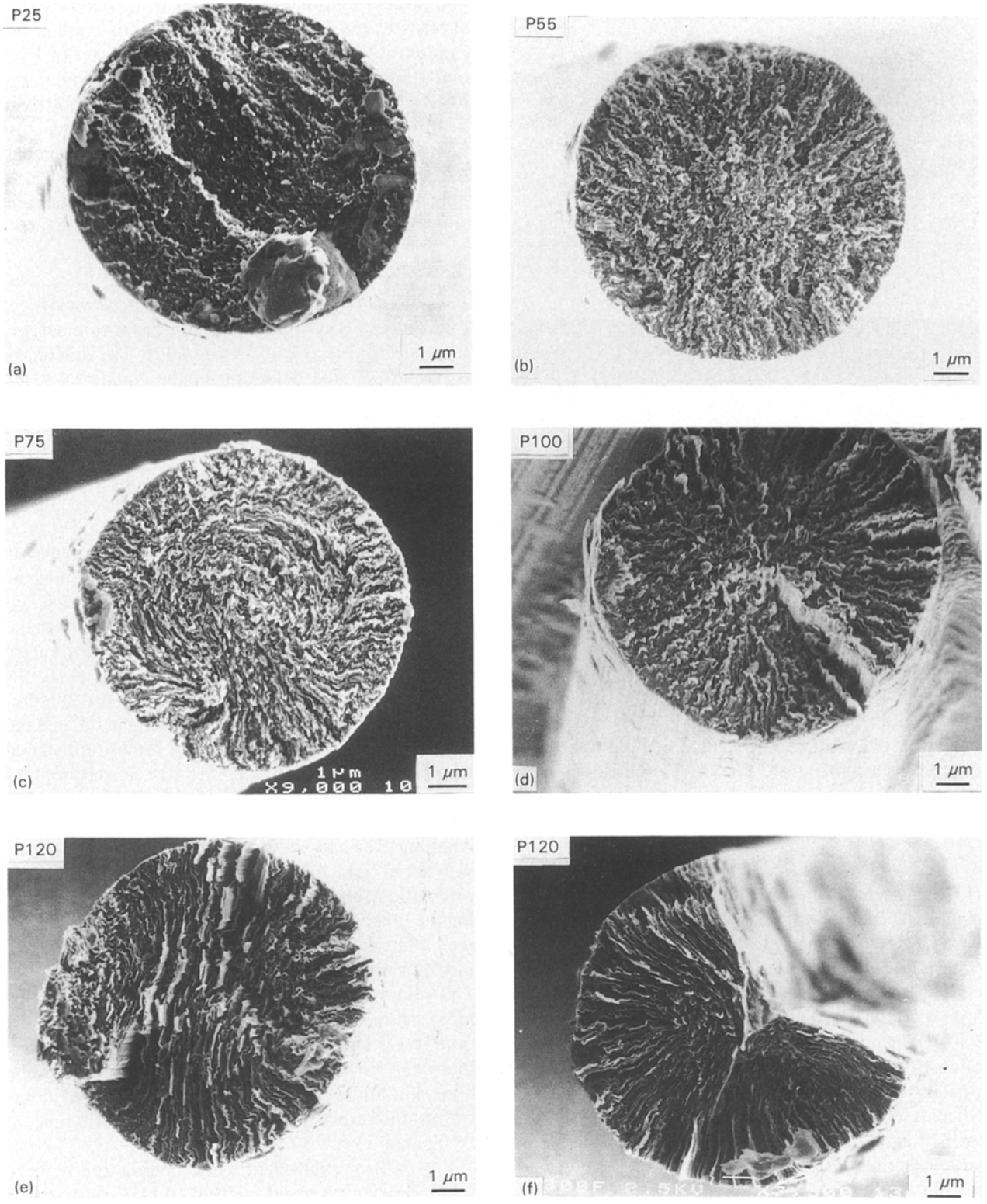

Figure 3 HRSEM micrographs of fracture surfaces of the mesophase pitch based carbon fibres. (a) P25, (b) P55, (c) P75, (d) P100, (e) P120 and (f) P120.

the graphite planes, unlike the case of the TEM observation of Guigon *et al.* [18]. In this case the width of the bright domains in the dark-field micrograph reflects the crystal size, L_c, and it is found to be in the range 10–80 nm with an average of ca. 35 nm, in good agreement with the X-ray diffraction measurements of L_c for this fibre (Table II). The voids separating the fibrils could either be true structural defects or thin cracks between the graphite planes formed during sectioning.

3.2. Mechanical testing

The tensile stress–strain curves for fibres P25, P55 and P75 are presented in Fig. 6, they show non-linear elastic behaviour with the slope of the curves tending

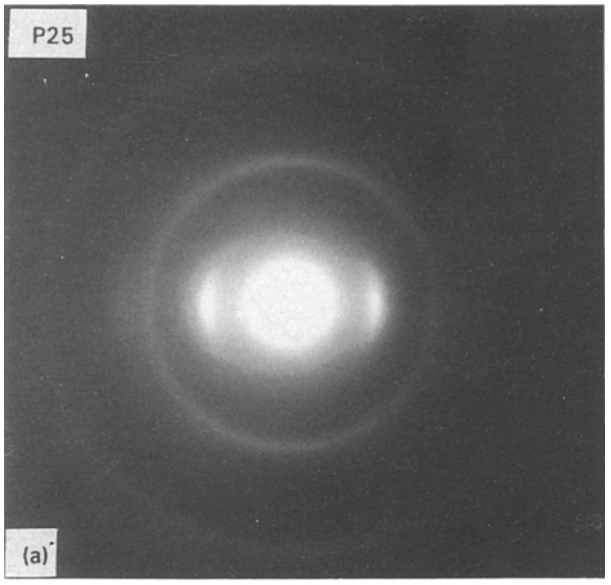

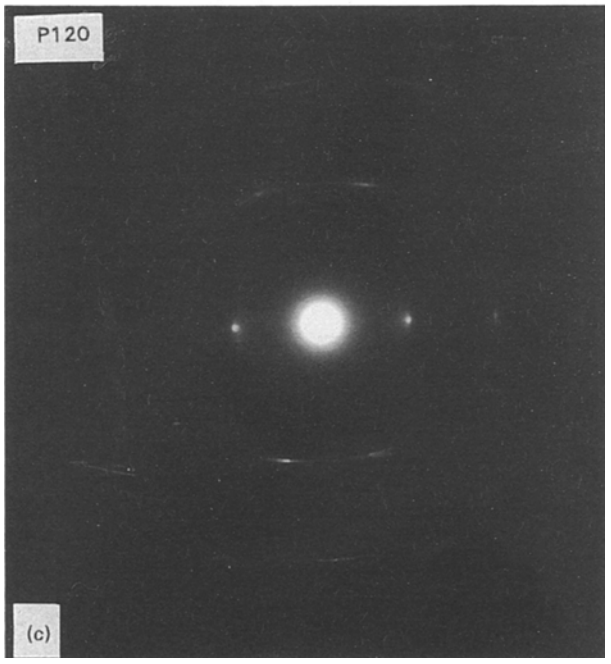

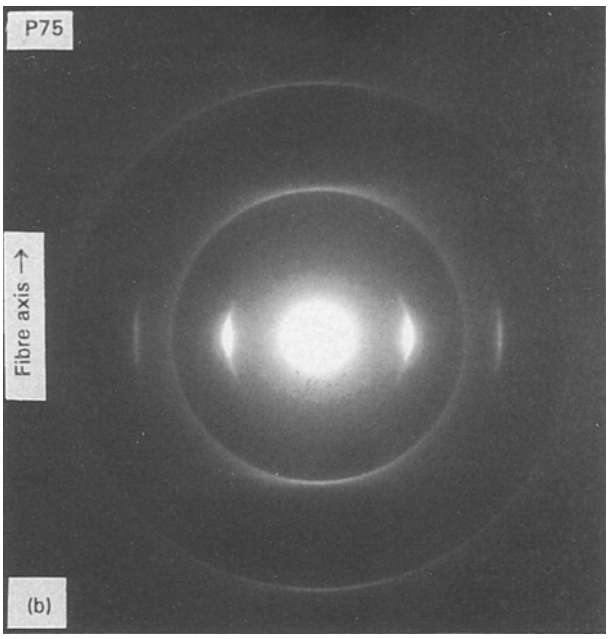

Figure 4 Selected-area diffraction patterns of (a) P25, (b) P75 and (c) P120 fibres.

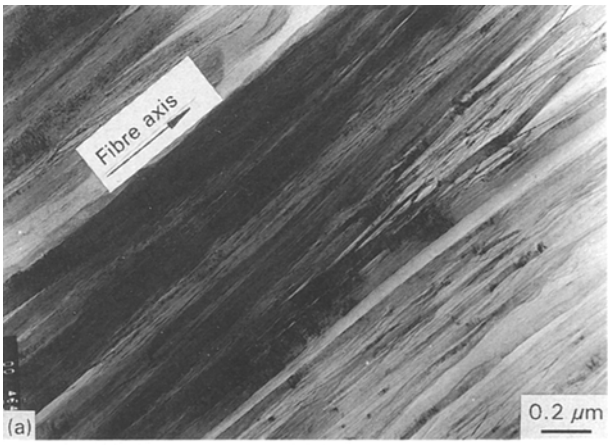

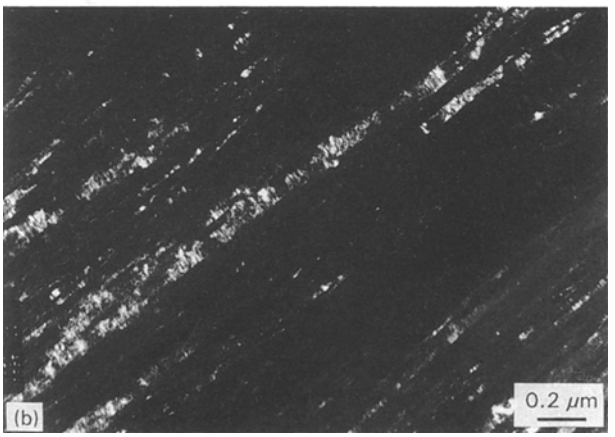

Figure 5 Transmission electron micrographs of microstructure of fibre P100, (a) bright-field image and (b) dark-field image.

to increase with increasing strain. Fig. 7 shows the dependence of the initial modulus of the fibres upon the gauge length and it can be seen that the measured modulus increases as the reciprocal of the gauge length decreases. This is thought to be due to a combination of machine softness and end effects, the effect is more pronounced for higher modulus fibres. Hence, the "true" value of the modulus can be determined by extrapolating the lines to infinite gauge length, as shown in Fig. 7. The values of the modulus obtained from such an extrapolation are close to those quoted by the manufacturers (Table I) determined using an aligned strand test on a tow of fibres impregnated with epoxy resin.

The variation of tensile strength with gauge length is plotted for the fibres in Fig. 8 in the form of a semi-log plot which shows approximately linear behaviour. The strong dependence of the tensile strength upon gauge length is due to the presence of defects and flaws [19, 20]. An estimate of the "intrinsic strength" of the fibres can be obtained by extrapolating to a small gauge length (ca. 0.3 mm) [5, 21] but the values of strength obtained are much higher than the manufacturer's quoted values (Table I). These were generally obtained using an aligned strand test on tow

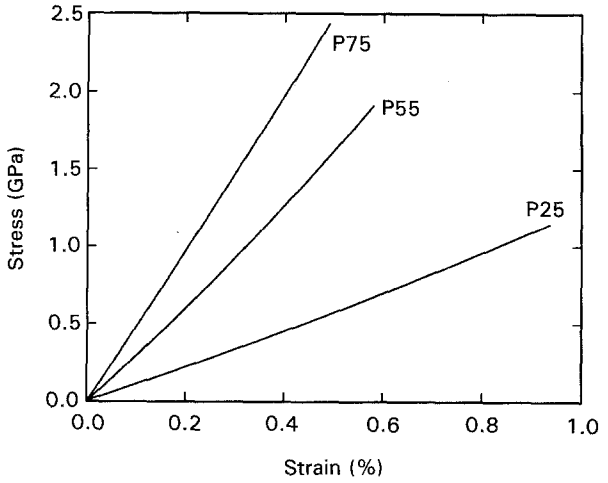

Figure 6 Stress–strain curves for single filaments of fibres P25, P55 and P75.

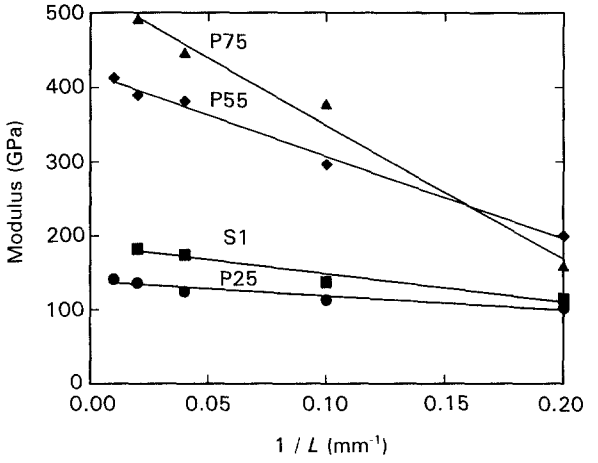

Figure 7 Dependence of the tensile modulus upon the reciprocal of the fibre gauge length for different fibres.

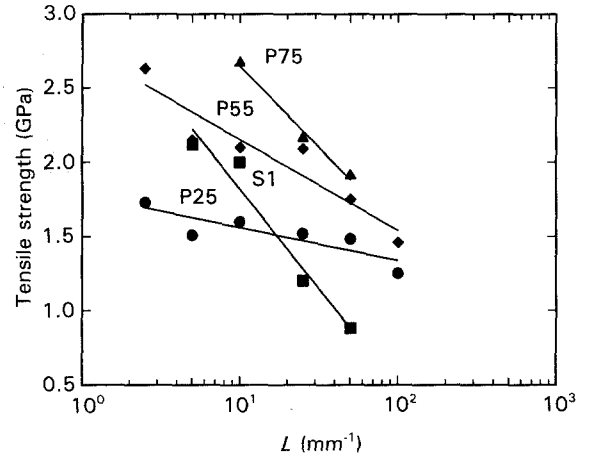

Figure 8 Dependence of the tensile strength upon gauge length for different fibres.

of fibres impregnated with resin. The effect of gauge length is not taken into account and Barr *et al.* [3] have shown that the values of tensile strength obtained by such a technique are significantly lower than those obtained using single-filament tests.

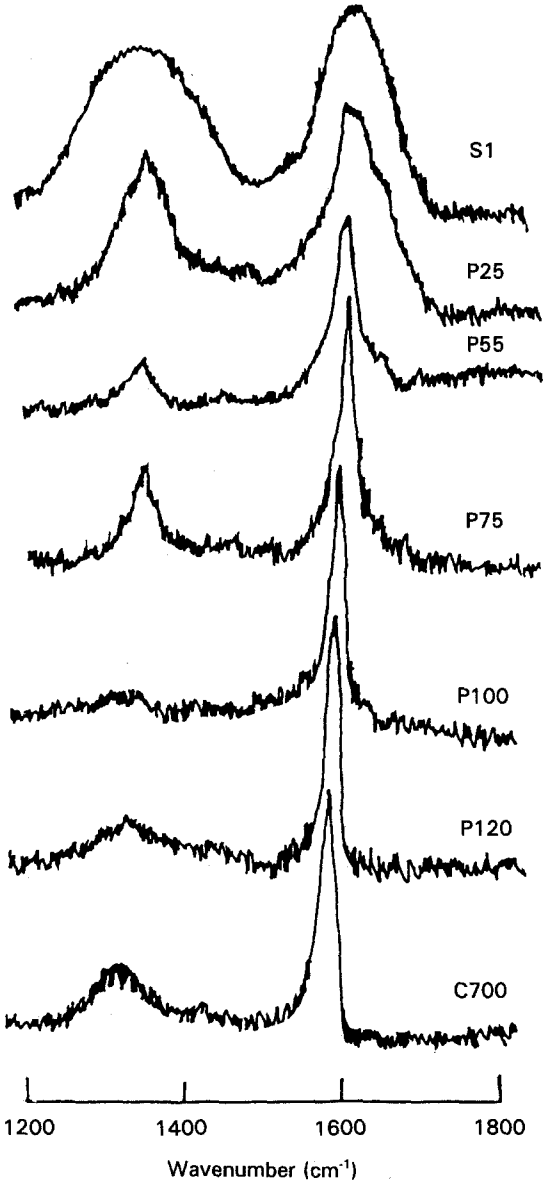

Figure 9 Raman spectra for all the mesophase pitch based fibres studied.

4. Raman spectroscopy

4.1. Raman spectra

It is well established that there are two first-order bands in the Raman spectra of carbon fibres [22]. One is ca. 1580 cm^{-1} and due to the in-plane stretching mode of the graphite planes and the other is at 1360 cm^{-1} which is thought to be due to the crystal boundary regions. The Raman spectra in the region 1200–1800 cm^{-1} for all of the pitch-based carbon fibres studied are given in Fig. 9. Significant differences can be seen for the spectra from the different fibres and it can be seen that the relative intensity of the 1360 cm^{-1} band decreases with respect to that of the 1580 cm^{-1} band as the crystal modulus increases. Tuinstra and Koenig [23] showed that the relative intensity of these two bands, I_{1360}/I_{1580}, is inversely proportional to the crystal size, L_a, determined using WAXD. An important point to note is that X-ray diffraction determines the average crystal size for the whole of the fibres whereas Raman spectra are obtained only from the surface regions of the fibres up to a few thousand nm deep [23, 24]. Hence, Raman

spectroscopy can be used to quantify differences in microstructure between skin and core regions of fibres by sectioning embedded fibres [25]. Significant differences between spectra obtained from the skin and core regions of the PAN-based carbon fibres are found but not for the pitch-based fibres. This is consistent with similar SAD patterns from the skin and core regions of the pitch-based fibres (Section 3.1.4).

As well as differences in Raman band intensity, Fig. 9 also shows that the band peak positions move to lower frequencies and the band widths decrease as the fibre modulus increases [26]. In addition, it can be seen that there is an extra shoulder at 1620 cm^{-1} for P25. This is thought to arise from structural disorder in the material [24, 27, 28] and coincides with the presence of a long tail for the (0 0 2) Bragg peak in the X-ray diffraction pattern (Fig. 1).

4.2. Effect of deformation upon the Raman spectra

The effect of deformation of graphite and carbon fibres produced from different precursors has been studied by Raman spectroscopy [29–31]. It is found that the band at 1580 cm^{-1} shifts to a lower frequency on the application of tensile stress or strain and that the position of the band at 1360 cm^{-1} is also sensitive to changes in stress or strain. The band at 1360 cm^{-1}, however, becomes less well-defined for fibres with higher values of Young's modulus and so the systematic study described here is concerned only with the strain sensitivity of the band at 1580 cm^{-1}. Fig. 10 shows the 1580 cm^{-1} band for a P75 fibre in the undeformed state and at a tensile strain of 0.44%. A clear shift to a lower frequency can be seen and Fig. 11 shows the dependence of the peak position upon strain for the pitch-based fibre of different moduli. It can be seen that the slopes of the lines in Fig. 11 increase with increasing fibre modulus showing that the Raman bands for the higher modulus fibres have a higher strain sensitivity. Fig. 12 shows the slope of the lines in Fig. 11 plotted as a function of fibre modulus and it can be seen that there is an approximately linear dependence implying that for a given level of strain there is more deformation of the graphite planes in the higher modulus fibres. This behaviour is similar to that of aramid fibres where a similar dependence of the rate of Raman band shift upon fibre modulus is obtained [15, 32]. Larger levels of shift per unit strain for higher modulus fibres have also been reported for rigid-rod polymer fibres [33] and for gel-spun polyethylene [34, 35]. The behaviour shown in Fig. 12 is crucial in understanding the relationship between structure and mechanical properties for carbon fibres, described in Section 5.

5. Dependence of mechanical properties upon fibre structure

5.1. Tensile modulus

It is generally accepted that the modulus of high-performance fibres is related to the degree of molecular orientation in the fibres, with the highest modulus fibres having the highest levels of molecular orientation [15]. Attempts have been made to explain the relationship between the tensile modulus and orientation by relating the elastic behaviour to the elastic constants of single crystals of graphite [36, 37] using both uniform stress and uniform strain models, whereby the fibres are considered to be composed of

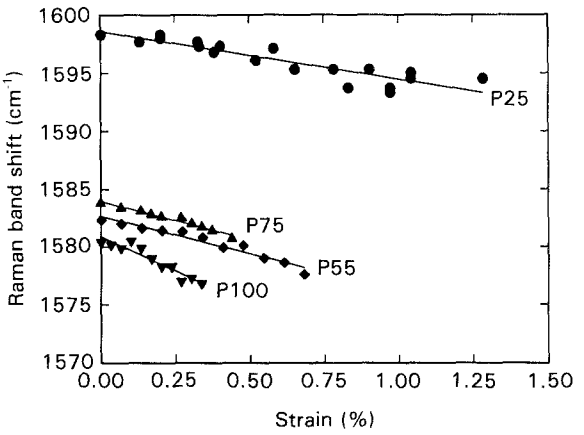

Figure 11 The variation of band position with strain for fibres P25, P55, P75 and P100.

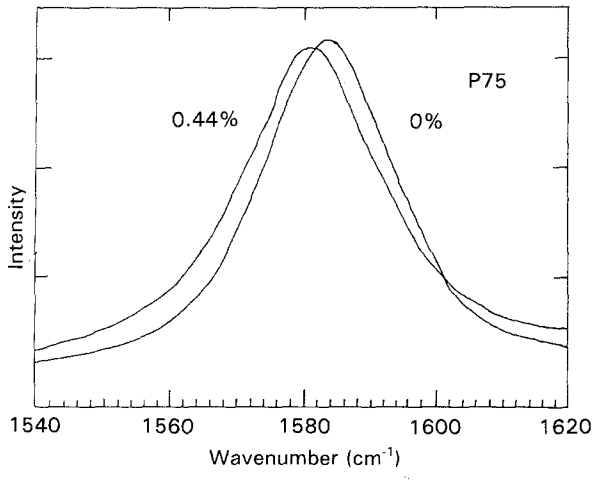

Figure 10 Difference in position of the Raman band 1580 cm^{-1} at 0 and 0.44% strain for P75.

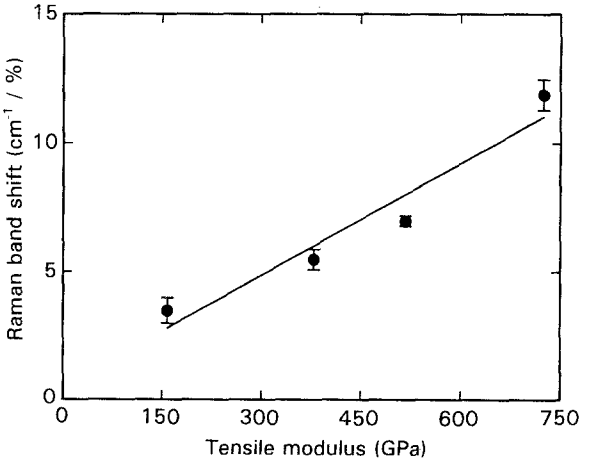

Figure 12 The dependence of the rate of Raman band shift per unit strain upon Young's modulus for the different fibres studied.

relatively-perfect graphite crystals with a range of orientations with respect to the fibre axis.

Northolt *et al.* [38] developed this approach and showed that the uniform stress model could be used to describe quantitatively the dependence of tensile modulus upon orientation. They showed that the relationship between the Young's modulus, E, of the fibres and the orientation is given by a relationship of the form

$$\frac{1}{E} = \frac{1}{E_c} + \frac{\langle\cos^2\phi\rangle}{G_c} \quad (1)$$

where E_c is the axial crystal modulus, G_c is the axial shear modulus and $\langle\cos^2\phi\rangle$ is the orientation parameter determined using X-ray diffraction or, in this case, electron microscopy.

It is known [38] that the intensity distribution of the (0 0 2) diffraction peak can be fitted to a Gaussian distribution and that the orientation parameter $\langle\cos^2\phi\rangle$ can be expressed with respect to the half-width at half-maximum, θ_h, for the peak as

$$\langle\cos^2\phi\rangle = 0.722 \sin^2\theta_h \quad (2)$$

The porosity of the fibres also affects the mechanical properties since the voids do not make any contribution to load bearing and so reduce the effective cross-sectional area such that the corrected value of Young's modulus is given by

$$E_{corr} = \frac{d}{d_{graphite}} \times E \quad (3)$$

where E is the observed value of modulus, d is the measured fibre density and $d_{graphite}$ is the density of an ideal graphite crystal (ca. 2.23 g cm^{-3} [38]).

The reciprocal of the density-corrected value of Young's modulus, $1/E_{corr}$ is plotted against our values of $\langle\cos^2\phi\rangle$ (determined by electron diffraction) in Fig. 13 in accordance with Equation 1. It can be seen that $1/E_{corr}$ increases linearly with $\langle\cos^2\phi\rangle$ and an extrapolation of the linear plot to a zero value of $\langle\cos^2\phi\rangle$ (i.e. perfect orientation) gives a value of crystal modulus, E_c, of ca. 1290 GPa, which is close to the values of 1020 $\pm$ 30 GPa determined by Blakslee *et al.* [39] using an ultrasonic method and of 1160 GPa calculated by Spence [40].

The shear modulus, G_c, can also be estimated using Equation 1 from the slope of the line in Fig. 13. It is found to be ca. 15.8 GPa which is much higher than the value of 5.05 $\pm$ 0.35 GPa for graphite crystals [41]. However, the torsional modulus of mesophase pitch-based fibres was measured to be ca. 9–15 GPa by Hawthorne [42], which is in agreement with our derived value.

The data of Northolt *et al.* [38] for pitch-based fibres are also plotted in Fig. 13 using values of $\langle\cos^2\phi\rangle$ determined using X-ray diffraction. These data yield a value of crystal modulus of 776 GPa and a shear modulus of ca. 15 GPa. The difference in the results obtained by the two methods could be due to the different methods of determining $\langle\cos^2\phi\rangle$, i.e. X-ray diffraction and electron diffraction. A similar difference has been found for similar measurements on aramid fibres [15]. The values of θ_h determined in the present study were not corrected for instrumental broadening. The values of the half-width at half-maximum intensity for the (0 0 2) peak have been measured for our set of P-series fibres by Arsenovic *et al.* [43] using X-ray diffraction, their values were ca. 3–4° lower than our electron diffraction values. This systematic error would tend to make our values closer to those of Northolt et al. [38] in Fig. 13.

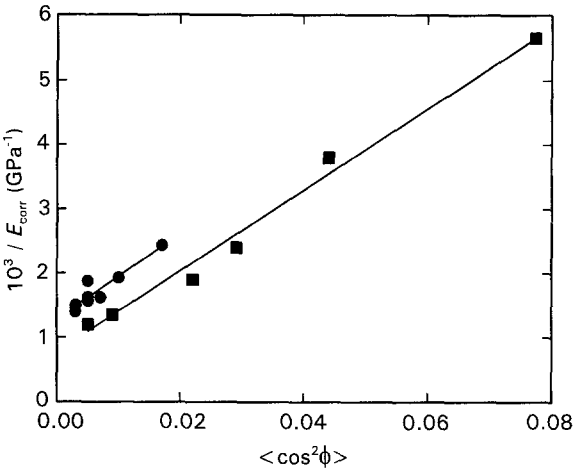

Figure 13 The dependence of the reciprocal of the corrected Young's modulus, $1/E_{corr}$, upon orientation parameter, $\langle\cos^2\phi\rangle$ for the different fibres studied (●, data from Ref. 38).

The results in Fig. 13 are also in qualitative agreement with the deformation studies using Raman spectroscopy described in Section 3.2. The strain-induced Raman band shifts are essentially a measure of the crystal stretching and not crystal rotation. Hence it is expected that in the higher modulus fibres there is more crystal stretching per unit strain and so the dependence of the rate of Raman band shift upon fibre modulus found in Fig. 12 is predicted.

5.2. Fracture behaviour

Although it is known that the presence of flaws in the structure limits the strength of materials the relationship between the microstructure and tensile strength of carbon fibres is not yet fully understood. Bennett *et al.* [44] found that flaws such as large misoriented crystals, rather than holes, limit the strength of PAN-based carbon fibres. Mesophase pitch-based carbon fibres generally have poorer levels of tensile strength than PAN-based fibres with the same values of modulus, probably due to their sheet-like structure (Fig. 3) which allows easy formation and propagation of transverse cracks.

Fig. 14 shows the dependence of the strain-to-failure of the fibres upon the d_{002} crystal spacing for the fibres investigated in this present study. Recent studies by Kumar *et al.* [45] have shown a strong relationship between carbon fibre compressive strength and the crystalline structure. The (0 0 2) d-spacings for the same set of pitch-based fibres determined from WAXD by them are in excellent agreement with this data, although their work was carried out on fibre bundles whilst ours was performed upon ground-up samples. The data of Endo [10] for pitch-based fibres are also included in Fig. 14, along with

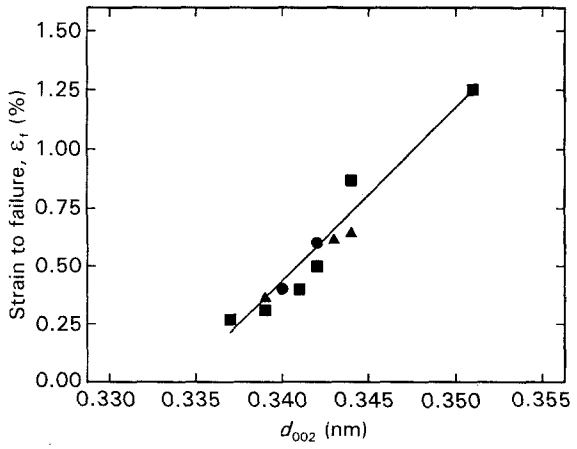

Figure 14 The dependence of the strain to failure, e_f upon d_{002} spacing for the different fibres studied. (●, Endo data from Ref. 11; ▲, PAN-based fibres from Ref. 25).

our data from PAN-based fibres [25], it can be seen that all of the data fall approximately on a straight line. This shows the direct effect of the fibre microstructure upon fracture behaviour. The decrease in the value of d_{002} is a reflection of an increase in the crystal perfection and it can be seen that this leads to a reduction in failure strain. In the more highly-graphitized fibres, such as P120, the HRSEM micrograph (Fig. 3) shows that the graphite planes are almost flat, whereas in less graphitized fibres they are more folded leading to a lower value of d_{002}. Hence, it seems that crack propagation will be more difficult in the less perfect structure leading to a higher strain to failure. The effect of this microstructure upon the strength of the fibres is more complex since it depends upon both the fibre modulus and strain to failure such that the fibres with the best levels of strength will have both a high modulus and a high strain to failure.

6. Conclusions

It has been shown that Raman spectroscopy is a powerful technique to both characterize the structure of carbon fibres and to follow the micromechanics of fibre deformation. The 1580 cm^{-1} Raman band moves to a lower frequency under the action of tensile deformation and the rate of shift of the band per unit strain increases linearly with the Young's modulus of the fibres.

It has been also shown that the tensile modulus of the mesophase pitch-based carbon fibres can be increased by increasing the degree of molecular orientation. This improved orientation, however, leads to the formation of larger, less-folded graphite sheets which can reduce the strain to failure of the fibres.

Acknowledgements

This work was supported by research grant from the SERC and the MOD. One of us (RJY) is grateful to the Royal Society for support in the form of the Wolfson Research Professorship in Materials Science. The authors are also grateful to I. Brough of the Manchester Materials Science Centre and A. Yarwood of JEOL (UK) Ltd for help with the HRSEM work and to Dr W. W. Adams of the USAF Wright Laboratory for supplying fibres.

References

1. L. S. SINGER, *Carbon* **16** (1970) 409.
2. L. S. SINGER, Belgian Patent 797,543 (1973).
3. J. B. BARR, S. CHWASTIAK, R. DIDCHENKO, I. C. LEWIS, R. T. LEWIS and L. S. SINGER, *Appl. Polym. Symp.* **29** (1976) 161.
4. H. FUJIMAKI, F. KODAMA, K. OKUDA, Y. SAKAGUCHI and S. OTANI, *Tanso* **80** (1975) 3.
5. J. D. H. HUGHES, *J. Phys. D: Appl. Phys.* **20** (1987) 276.
6. R. BACON and W. A. SCHALAMON, in 5th Biennial Conference on Carbon, Buffalo, NY (1967).
7. W. WATT and W. JOHNSON, in Proceedings of the Third Conference on Ind. Carbon and Graphite (Soc. Chem. Ind., London, 1971) p. 417.
8. S. ALLEN, G. A. COOPER, D. J. JOHNSON and R. M. MAYER, *ibid.* (1971) p. 456.
9. D. L. VEZIE and W. W. ADAMS, *J. Mater. Sci. Lett.* **9** (1990) 883.
10. M. GUIGON and A. OBERLIN, *Comp. Sci. Technol.* **25** (1986) 231.
11. M. ENDO, *J. Mater. Sci.* **23** (1988) 598.
12. B. BRIGHT and L. S. SINGER, *Carbon* **17** (1979) 59.
13. T. HAMADA, T. NISHIDA, M. FURUYAMA and T. TOMIOKA, *Carbon* **26** (1988) 837.
14. T. MATSUMOTO, *Pure Appl. Chem.* **57** (1985) 1553.
15. R. J. YOUNG, D. LU, R. J. DAY, W. F. KNOFF and H. A. DAVIS, *J. Mater. Sci.* **27** (1992) 5431.
16. W. RULAND, in Conference on Fibres for Composites (IPPI, Brighton, 1969).
17. D. J. JOHNSON and W. N. TYSON, *Brit. J. Appl. Phys.* (D) Ser 2.2 (1969) 787.
18. M. GUIGON, A. OBERLIN and G. DESARMOT, *Fibre Sci. Technol.* **20** (1984) 177.
19. J. W. JOHNSON, *Appl. Polym, Symp.* **9** (1969) 229.
20. R. MORETON, *Fibre Sci. Technol.* **1** (1968) 273.
21. J. B. JONES, J. B. BARR and R. E. SMITH, *J. Mater. Sci.* **15** (1980) 2415.
22. F. TUINSTRA and J. L. KOENIG, *J. Chem. Phys.* **53** (1970) 1126.
23. F. TUINSTRA and J. L. KOENIG, *J. Comp. Mater.* **4** (1970) 492.
24. K. MORITA, Y. MURATA, A. ISHITANI, K. MURAYAMA, T. ONO and A. NAKAJIMA, *Pure Appl. Chem.* **58** (1986) 455.
25. Y. HUANG, J. BOON and R. J. YOUNG, in Proceedings of Fifth International Composite Conference on Fibre Reinforced Composites, University of Newcastle upon Tyne (PRI, 1992) 17/1.
26. E. FITZER, E. GANTNER, F. ROZPIOCH and D. STEINER, *High Temperature–High Pressure* **19** (1987) 537.
27. R. J. NEMANICH and S. A. SOLIN, *Phys. Rev.* **B20** (1979) 392.
28. G. KATAGIRI, H. ISHIDA and A. ISHITANI, *Carbon* **26** (1988) 565.
29. I. M. ROBINSON, M. ZAKIKHANI, R. J, DAY, R. J. YOUNG and C. GALIOTIS, *J. Mater. Sci. Lett.* **6** (1987) 1212.
30. H. SAKATA, G. DRESSELHAUS and M. ENDO, in Proceedings of the Eighteenth Carbon Conference (Worcester Polytechnic Institute, Worcester, MA, USA, 1987) p. 18.
31. C. GALIOTIS and D. N. BATCHELDER, *J. Mater. Sci. Lett.* **7** (1988) 545.
32. S. VAN DER ZWAAG, M. G. NORTHOLT, R. J. YOUNG, C. GALIOTIS, I. M. ROBINSON and D. N. BATCHELDER, *Polym. Comm.* **28** (1987) 276.
33. R. J. DAY, I. M. ROBINSON, M. ZAKAKHANI and R. J. YOUNG, *Polymer* **28** (1987) 1883.
34. B. J. KIP, M. C. P. VAN EIJK and R. J. MEINER, *J. Polym. Sci. Polym. Phys.* **29** (1991) 99.
35. K. PRASAD and D. T. GRUBB, *ibid.* **27** (1989) 381.

36. W. RULAND, *Appl. Polym. Symp.* **9** (1969) 293.
37. W. T. BRYDGES, D. V. BADAMI, J. C. JOINER and G. A. JONES, *ibid.* (1969) 255.
38. M. G. NORTHOLT, L. H. VELDHUZEN and H. JANSEN, *Carbon* **29** (1991) 1267.
39. O. L. BLAKSLEE, D. G. PROCTOR, E. J. SELDIN, G. B. SPENCE and T. WENG, *J. Appl. Phys.* **41** (1970) 3373.
40. G. B. SPENCE, in Proceedings of the Fifth Conference on Carbon (Pergamon Press, NewYork, 1961) Vol. 2, p. 531.
41. M. GRIMSDITCH, *J. Phys. C: Solid State Phys.* **16** (1983) L143.
42. H. M. HAWTHORNE, "Carbon fibres, their composites and applications" (The Plastics Institute, London, 1971) p. 81.
43. I. P. ARSENOVIC, H. JIANG, R. E. EBY, W. ADAMS and J. M. JIU, in "Carbon 88", edited by B. McEnany and T. V. Mays (IOP Publishing Ltd, Bristol, 1988) p. 485.
44. S. C. BENNETT, D. J. JOHNSON and W. JOHNSON, *J. Mater. Sci.* **18** (1983) 3337.
45. S. KUMAR, D. P. ANDERSON and A. S. CRASTO, *J. Mater. Sci.* **28** (1993) 423.

Received 2 April 1993
and accepted 3 February 1994